Soft Matter

PAPER

View Article Online
View Journal | View Issue

Cite this: *Soft Matter*, 2023, **19**, 1966

Transition of rupture mode of strain crystallizing elastomers in tensile edge-crack tests†

Katsuhiko Tsunoda,*[a] Yuji Kitamura[b] and Kenji Urayama *[c]

We revisit the classical results that the fracture energy density (W_b) of strain crystallizing (SC) elastomers exhibits an abrupt change at a characteristic value (c_0^*) of initial notch length (c_0) in tensile edge-crack tests. We elucidate that the abrupt change of W_b reflects the transition in rupture mode between the catastrophic crack growth without a significant SIC effect at $c_0 > c_0^*$ and the crack growth like that under cyclic loading (dc/dn mode) at $c_0 < c_0^*$ as a result of a pronounced SIC effect near the crack tip. At $c_0 < c_0^*$, the tearing energy (G) was considerably enhanced by hardening *via* SIC near the crack tip, preventing and postponing catastrophic crack growth. The fracture dominated by the dc/dn mode at $c_0 < c_0^*$ was validated by the c_0-dependent G characterized by $G = (c_0/B)^{1/2}/2$ and the specific striations on the fracture surface. As the theory expects, coefficient B quantitatively agreed with the result of a separate cyclic loading test using the same specimen. We propose the methodology to quantify the tearing energy enhanced *via* SIC (G_{SIC}) and to evaluate the dependence of G_{SIC} on ambient temperature (T) and strain rate ($\dot{\varepsilon}$). The disappearance of the transition feature in the W_b–c_0 relationships enables us to estimate definitely the upper limits of the SIC effects for T (T^*) and $\dot{\varepsilon}$ ($\dot{\varepsilon}^*$). Comparisons of the G_{SIC}, T^*, and $\dot{\varepsilon}^*$ values between natural rubber (NR) and its synthetic analog reveal the superior reinforcement effect *via* SIC in NR.

Received 17th January 2023,
Accepted 7th February 2023

DOI: 10.1039/d3sm00060e

rsc.li/soft-matter-journal

Introduction

Natural rubber (NR) is one of the most widely used biomaterial polymers. NR has attracted increasing interest in environmental issues and momentum toward realizing a sustainable society.[1–3] A unique feature of NR is strain-induced crystallization (SIC): NR undergoes partial crystallization when subjected to a sufficiently large strain.[4,5] SIC considerably hardens rubber, resulting in a marked stress-upturn in the stress–strain relationship. SIC is a self-reinforcement function that increases the tensile strength and fracture toughness. This beneficial feature distinguishes NR from other non-crystallizing (non-SIC) rubbers.[1–3] Synthetic *cis*-1,4-polyisoprene rubber (IR) is an NR analog. It has long been known that IR is appreciably inferior to NR in several SIC properties, such as the onset strain and the mechanical reinforcement effect.[6–9] The superior SIC abilities of NR relative to IR are often attributed to the perfect stereoregularity of *cis*-1,4-polyisoprene and a pseudo-network *via* the interaction between the end-functional groups in the rubber chains and non-rubber components such as fatty acids, proteins, and lipids.[10–13] Recently, it has been reported that SIC can occur even in gels with high solvent contents, significantly enhancing the mechanical toughness.[14] SIC has received considerable interest as a key for toughening not only rubbers but also gels.

The SIC near the crack tip subjected to large deformation contributes to enhancing the tear strength or suppressing the catastrophic crack growth.[15–20] The SIC near the crack tip was revealed by investigations using the micro-beam wide-angle X-ray scattering (WAXS) technique.[21,22] However, many aspects of the reinforcement effects *via* SIC remain to be quantified. The reinforcement effect *via* SIC is expected to have an upper limit for each ambient temperature (T) and imposed strain rate ($\dot{\varepsilon}$) (designated as T^* and $\dot{\varepsilon}^*$, respectively), because the crystal has a melting temperature and SIC is a kinetic event. The melting temperatures (T_f) of the SIC crystals of NR and IR were investigated using WAXS experiments in the stretched state at various T.[23–29] The T_f increased with imposed stretch reflecting an increase in the crystallinity index, which was thermodynamically explained by a reduction in the configurational entropy of network strands.[1–3,30] T_f is an equilibrium property,

[a] *Sustainable and Advanced Materials Division, Bridgestone Corporation, Tokyo 187-8531, Japan. E-mail: katsuhiko.tsunoda@bridgestone.com*
[b] *Sustainable and Advanced Materials Division, Bridgestone Corporation, Tokyo 187-8531, Japan*
[c] *Department of Material Chemistry, Graduate School of Engineering, Kyoto University, Kyoto 615-8510, Japan. E-mail: urayama.kenji.2s@kyoto-u.ac.jp*

† Electronic supplementary information (ESI) available: Tensile force–displacement curves for NR-B with various c_0 values at 25 °C with a strain rate of 0.11 s^{-1} in the edge-crack test. See DOI: https://doi.org/10.1039/d3sm00060e

while the SIC kinetics is significantly affected by the ambient temperature (T). At T^* the SIC kinetics becomes so slow that SIC cannot occur at $\dot{\varepsilon}$ of interest.

The effect of $\dot{\varepsilon}$ on SIC was examined by WAXS experiments using custom-made tensile instruments that could achieve high strain rates. The upper limit $\dot{\varepsilon}$ for SIC remains unclear because finite SIC was still observed at high strain rates on the order of 10^2 s^{-1}.[31–35] The reinforcement effect *via* SIC is expected to depend on T and $\dot{\varepsilon}$ and to disappear at sufficiently high T or $\dot{\varepsilon}$ exceeding T^* and $\dot{\varepsilon}^*$. However, in general, the evaluations of T^* and $\dot{\varepsilon}^*$ in conventional tensile tests using unnotched bulk specimens involve appreciable ambiguity, because the tensile strength (stress at break) data as a function of T or $\dot{\varepsilon}$ often show scattering owing to the high susceptibility to inherent flaws.[36]

The evaluation of the tearing energy, which is the energy required for crack propagation at given T and $\dot{\varepsilon}$, in rubber-like materials has attracted considerable interest since tearing energy is a key property to characterize the fracture behavior.[37–45] A classical tensile fracture test, called the "edge-crack test," provides an important basis for characterizing the reinforcement effect *via* SIC.[36,46–48] Thomas *et al.*[36,46,47] and Hamed *et al.*[48] investigated the strain energy density at break (W_b) for pre-notched NR specimens as a function of the initial notch length (c_0) through tensile experiments. They found that W_b decreased with increasing c_0, but with an abrupt fall at a characteristic c_0 value (c_0^*), whereas this abrupt change was not observed for non-SIC rubber. They regarded this discontinuity as a transition between the tensile fractures with or without a significant SIC effect; at $c_0 < c_0^*$, a sufficiently wide region near the crack tip underwent SIC, resulting in an enhancement of W_b. Hamed *et al.* investigated the influence of cross-links and filler contents on the transition behavior of NR in edge-crack tests[49,50] and discussed the synergetic effects of SIC and filler loading.

In this study, we revisit the discontinuous W_b–c_0 relationships specific to the SIC rubbers and elucidate that the discontinuity results from the transition of rupture mode between the catastrophic crack growth without an appreciable SIC effect at $c_0 > c_0^*$ and the crack growth like that under cyclic loading (dc/dn mode) undergoing a significant SIC effect. The occurrence of the cyclic crack growth mode at $c_0 < c_0^*$ is validated by the characteristic striations on the fracture surface and the result of a separate cyclic loading test using the same specimen. We propose the methodology to quantify the tearing energy enhanced *via* SIC (G_{SIC}) from the W_b–c_0 data and to evaluate T^* and $\dot{\varepsilon}^*$ from the disappearance of the transition feature. We demonstrate that the comparisons of the G_{SIC}, T^*, and $\dot{\varepsilon}^*$ values between NR and IR reveal the superior reinforcement effect *via* SIC in NR.

Theory for the edge-crack test of SIC rubber

Crack growth in rubber has been successfully described using fracture mechanics based on the concept of tearing energy. Tearing energy, G, which is the required energy to drive a crack

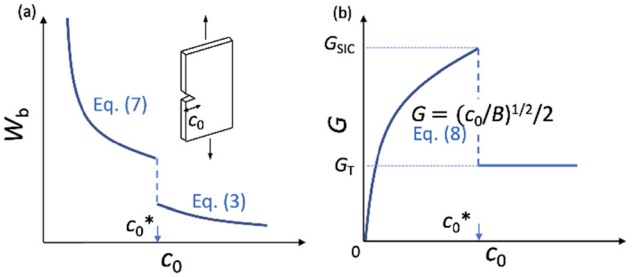

Fig. 1 Schematic illustrations of the theoretical relationships of (a) strain energy density at break (W_b) and initial notch length (c_0), and (b) tearing energy (G) and c_0. Crack growth of a single-edge crack specimen (inset) undergoes a transition between the catastrophic failure ($c_0 > c_0^*$) and the dc/dn mode ($c_0 < c_0^*$).

with a unit area in size, is defined as follows:[37,51]

$$G = -\frac{1}{t}\left(\frac{\partial U}{\partial c}\right)_l \quad (1)$$

where c is the length of a crack in a material with a thickness of t and U is the total strain energy. The differential is conducted at a constant specimen length (l) or constant strain. For a strip tensile specimen with an edge flaw of length (c) (inset of Fig. 1a), G is given by:[37]

$$G = 2kWc \quad (2)$$

where W is the strain energy density in the bulk specimen (far from the crack tip) and k is a slightly varying function of the extension ratio (λ), given by $k = \pi/\lambda^{1/2}$. The tearing energy, G, reflects the energy required to break the bonds across the fracture plane and the energy dissipated during fracture.

Eqn (2) was experimentally validated using the edge-crack test of non-SIC rubbers by varying the initial notch length (c_0):[52] the strain energy density at break (W_b) is simply proportional to ${c_0}^{-1}$, reflecting the fact that G is a material constant for non-SIC rubbers. By contrast, SIC rubbers exhibit a discontinuous transition in the W_b–c_0 relationships: W_b decreases with increasing c_0, and notably, W_b falls abruptly at a characteristic value of c_0 (c_0^*),[36,46–48] which is schematically shown in Fig. 1a. Thomas *et al.*[36,46,47] regarded this abrupt change in W_b at c_0^* as a transition in the rupture mechanism; at $c_0 > c_0^*$, no significant SIC occurs ahead of the advancing crack tip of the specimens, resulting in the catastrophic crack growth process observed in the non-SIC rubbers. At $c_0 < c_0^*$, a sufficiently large SIC region emerged near the crack tip, preventing or postponing the catastrophic crack growth process. At $c_0 > c_0^*$ without a significant SIC effect, when the failure follows the ordinary tearing mode, the c_0 dependence of W_b can be expressed by eqn (2) as follows:

$$W_b = \frac{G_T}{2kc_0} \quad \text{at } c_0 > c_0^* \quad (3)$$

where G_T is the critical tearing energy for the onset of catastrophic crack growth. If a specimen undergoes SIC in a sufficiently large area near the crack tip, the crack growth requires a higher G than the G_T because the crack propagates through the crystalline region. Thomas *et al.* assumed that the corresponding crack

propagates like crack growth under cyclic loading.[36,46,47] When the notch grows by Δc during the loading, G is given from eqn (2) as follows:

$$G = 2kW(c_0 + \Delta c) \quad (4)$$

In general, the crack growth rate during a loading cycle (dc/dn) is related to G by a power law according to Paris and Erdogan,[53] $\Delta c = dc/dn = BG^{\alpha}$, where B is the material constant related to the crack growth, which can be obtained by cyclic crack growth measurement under a large strain. In the case of NR, the power law with $\alpha = 2$ satisfactorily describes the behavior at moderate and high G values;[54] the relationship of current interest is written as follows:

$$\Delta c = BG^2 \quad (5)$$

The following relationship is obtained by eliminating G using eqn (4) and (5) as follows:

$$\Delta c = 4k^2B\,(c_0 + \Delta c)^2\,W^2 \quad (6)$$

Postulating that this quadratic equation for Δc has real solutions provides the condition that the crack grows indefinitely, that is, the rupture occurs.[46] The corresponding postulate gives W_b in the tensile fracture *via* the cyclic crack growth mode:

$$W_b = \frac{1}{4kc_0^{1/2}B^{1/2}} \quad \text{at } c_0 < c_0^* \quad (7)$$

The transition of the W_b–c_0 relationship between eqn (3) and (7) is schematically illustrated in Fig. 1a. Thomas and co-workers[36,46,47] explained the experimental data for NR at $c_0 > c_0^*$ and $c_0 < c_0^*$ using eqn (3) and (7), respectively.

The W_b values below c_0^* are significantly larger than those beyond c_0^*, reflecting the enhancement effect of SIC on the tearing energy. However, the corresponding effect is yet to be quantified from the W_b–c_0 data. Therefore, we extend the analysis to quantify the tearing energy enhanced by the SIC effect (G_{SIC}). Eqn (4) is expressed using eqn (7) by eliminating k as follows:

$$G = \frac{1}{2}\left(\frac{c_0}{B}\right)^{1/2}\left(1 + \frac{\Delta c}{c_0}\right) \approx \frac{1}{2}\left(\frac{c_0}{B}\right)^{1/2} \quad \text{at } c_0 < c_0^* \quad (8)$$

The increment Δc, which is characterized by the interval between adjacent striation lines in the fracture surface, is significantly smaller than c_0 (*i.e.*, $\Delta c/c_0 \ll 1$), as will be shown later. Eqn (8) (*i.e.*, $c_0 \approx 4BG^2$) expects that G increases proportionally to $c_0^{1/2}$ when $c_0 < c_0^*$, reflecting the feature of the dc/dn mode (eqn (5); $\Delta c = BG^2$). When c_0 exceeds c_0^*, G is expected to drop abruptly to G_T in eqn (3) because the fracture occurs *via* catastrophic crack growth (ordinary tear manner); there is no significant SIC near the crack tip. Fig. 1b schematically illustrates the c_0 dependence of G in this scenario. The maximum value of G at c_0^* can be regarded as the characteristic tearing energy enhanced by the SIC effect (G_{SIC}). In the case of non-SIC rubber, G in cyclic crack growth which is a subcritical process is significantly smaller than G_T. In the edge-crack tensile tests of SIC rubber, G in cyclic crack growth mode can be larger than G_T, because the SIC near the crack tip pronouncedly enhances G at $c_0 < c_0^*$ whereas it is suppressed at $c_0 > c_0^*$.

Investigations of the W_b–c_0 relationships with varying ambient temperatures (T) and strain rates ($\dot{\varepsilon}$) (Fig. 1a) provide a basis for discussing the effects of T and $\dot{\varepsilon}$ on G_{SIC}. In particular, the corresponding data also enable us to evaluate T^* and $\dot{\varepsilon}^*$ (the upper limits for the SIC effect on tearing energy) because at $T > T^*$ and $\dot{\varepsilon} > \dot{\varepsilon}^*$, the transition feature vanishes, and only the ordinary tearing mode ($G \approx G_T$; eqn (3)) appears over the entire c_0 range.

Experimental section

Materials

The following compositions were employed for the preparation of the specimens designated as NR-A and IR-A: NR rubber gum (ribbed smoked sheet, RSS#3) or IR gum (IR2200, ENEOS Material Co.), stearic acid (2 phr, *i.e.*, 2 g per 100 g of gum rubber), ZnO (5.0 phr), polymerized 2,2,4-trimethyl-1,2-dihydroquinoline (TMDQ, 0.3 phr), *N*-1,3-dimethylbutyl-*N*′-phenyl-*p*-phenylenediamine (6PPD, 1 phr), *N*-cyclohexyl-2-benzothiazole sulfenamide (CBS, 1.5 phr), and sulfur (1.5 phr).

First, gum, stearic acid, ZnO, TMQD, and 6PPD were mixed, and the mixture was sheared for 2 min in a chamber at a controlled temperature of 80 °C. Next, CBS and sulfur were added for vulcanization, and the mixtures were subjected to shear for 1.5 min at 80 °C. The mixtures were further sheared using an open-roll mill for 5 min at 60 °C. Finally, specimen sheets were prepared using a hot press method at 160 °C for 8 and 13 min for NR and IR, respectively. We used the NR-A and IR-A specimens for the edge-crack tests in order to investigate the enhancement effects *via* SIC on tearing energy at various T and $\dot{\varepsilon}$ values.

For comparing the results of the edge-crack and the cyclic loading tests, we employed the NR-B specimen which had almost the same compositions as NR-A but slightly differed in curatives: 1,3-diphenylguanidine (DPG, 0.35 phr), *N*-cyclohexyl-2-benzothiazole sulfenamide (CBS, 1.77 phr) and sulfur (1.4 phr). The processing procedure for the sheet specimens of NR-B was the same as that for NR-A.

NR-A and IR-A exhibited the same magnitudes of equilibrium swelling in toluene within the experimental error, indicating that they have similar cross-link densities. The average molecular weights between neighboring cross-links were estimated to be 7200 g mol^{-1} for NR-A and IR-A and 6400 g mol^{-1} for NR-B from the equilibrium swelling degrees using the Flory–Rehner equation.[55]

A styrene butadiene rubber (SBR) specimen was prepared as a non-SIC rubber for comparison, using SBR gum (#1500, ENEOS Material Co.). The compositions of stearic acid, ZnO, TMQD, 6PPD and sulfur were identical to those of NR-A. Diphenyl guanidine (1 phr), 2-benzothiazolyl disulfide (0.6 phr), and *N*-oxydiethylene-2-benzothiazole sulfenamide (0.6 phr) were used as cure accelerators. The specimen sheets were made using the same method as for NR-A at 160 °C for 6 min.

Edge-crack test

A tensile strip specimen (5 mm wide × 50 mm high × 2 mm thick) was used. An initial crack was inserted into the center of

a single side of the tensile strip specimen using a specially designed cutting apparatus. The initial crack length (c_0) was varied from 0.25 to 3.5 mm in an approximately 0.25 mm interval. Tensile measurements were performed using a tensile testing machine (Shimadzu AGX-Plus 1 kN and Hydroshot 1 kN) equipped with a controlled temperature chamber. To investigate the effect of T, T was varied from 25 °C to 90 °C, and the measurements were conducted at a fixed strain rate of 0.5 s^{-1}. To examine the effect of $\dot{\varepsilon}$, $\dot{\varepsilon}$ was varied from 0.005 to 500 s^{-1} at 25 °C.

The tensile force at break (f_b) of a pre-notched specimen with an initial notch length (c_0) was measured under the given conditions of T and $\dot{\varepsilon}$. The tearing energy (G) was calculated using eqn (2) corresponding to eqn (4) with $\Delta c/c_0 \ll 1$. The strain energy density at break (W_b) and λ in eqn (2) were obtained with the f_b value using the W–σ and σ–λ relationships for the corresponding unnotched bulk specimen.

Cyclic loading test

A cyclic loading test was conducted for the pre-notched NR-B specimens (5 mm wide × 50 mm high × 2 mm thick) using a tensile tester (Shimadzu AGX-Plus 1kN). The c_0 values were varied from 0.3 to 1.0 mm. The tensile specimen was cyclically loaded and unloaded between the desired extension length and zero position for 5 to 10 cycles at a crosshead speed of 200 mm min^{-1} and at 25 °C. The maximum stretch was varied between 3.6 and 7.0 depending on the pre-notch length of each specimen. The maximum force during each cycle was recorded, enabling the evaluation of the elastically stored energy density (W_i) and strain function (k_i) for the i-th cycle, using the W–σ and σ–λ relationships for the unnotched bulk NR-B specimen. After the cyclic loading test, the initial crack length (c_0) and the increment of crack length (Δc_i) in each cycle were precisely measured utilizing a digital video microscope as described below.

Observation of the fracture surface

The fracture surface of the specimens was observed using a digital microscope (Hi-rox Co., RH-2000) equipped with a variable lighting adopter. The c_0 values were measured from the fracture surface.

Wide-angle X-ray scattering measurements

WAXS measurements for the unnotched bulk NR-A and IR-A specimens were performed using synchrotron radiation at beamline BL03XU of SPring-8 (JASRI). The X-ray wavelength was 0.1 nm, and the camera length was 130 mm. A CMOS camera (Hamamatsu Photonics K.K. Orca Flash-4.0) equipped with an image intensifier was used as the detector. Specially designed in-house dumbbell specimens were stretched at a strain rate of 0.1 s^{-1}. Sequential WAXS images during the stretching process were recorded every second after the sample extension started. The X-ray scattering intensity at scattering vector q as a function of stretch (λ), $I_x^{obs}(q, \lambda)$, was obtained from the two-dimensional WAXS image by integrating $\beta = \pm 10°$ (β: azimuth angle) after correcting for the effects of the dark noise of the detector, air scattering, and sample thickness. Because no reflection from the SIC crystals was observed at $\lambda < 2$, the corresponding scattering intensity, $I_x^{OBS}(q, \lambda < 2)$, was regarded as the contribution from the amorphous phase. The scattering intensity from SIC crystals, I_x, was evaluated as follows:

$$I_x(q, \lambda) = I_x^{OBS}(q, \lambda) - I_x^{OBS}(q, \lambda < 2) \quad (9)$$

We employed the peak intensity of the crystal (200) diffraction (I_{200}) as a simple measure of the crystallinity index *via* the SIC.

Results and discussion

Non-SIC rubber in the edge-crack test

Fig. 2a illustrates W_b as a function of c_0 for a non-SIC rubber, styrene butadiene rubber (SBR), at 25 °C and a strain rate of 0.60 s^{-1} obtained using the edge-crack test. W_b decreased monotonically with increasing c_0. The G values calculated using the W_b data and eqn (2) are constant in the range of $c_0 \leq$ 3.55 mm examined here (Fig. 2b). It is naturally expected because G for the non-SIC rubber can be assumed as a c_0-independent critical tearing energy (G_T) for the onset of catastrophic crack growth at given T and $\dot{\varepsilon}$. Importantly, the

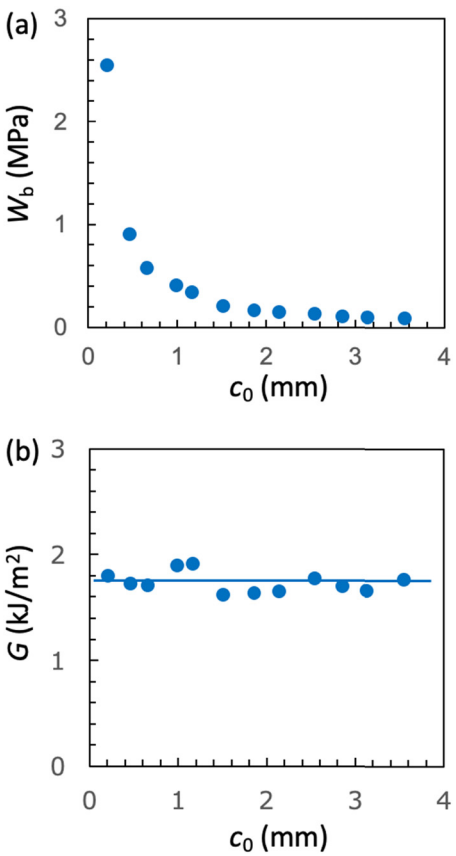

Fig. 2 (a) Strain energy density at break (W_b) as a function of the initial notch length (c_0) for SBR (non-SIC rubber) at 25 °C and a strain rate of 0.60 s^{-1} in the edge-crack test. (b) The c_0 dependence of tearing energy (G) calculated using the data in (a) with eqn (2).

constancy of G also validates the applicability of eqn (2) in the calculation of G for the specimens of $c_0 \leq 3.55$ mm in this experiment.

SIC rubber in the edge-crack test

Fig. 3a shows the plots of W_b *versus* c_0 for a SIC rubber, NR-B, at 25 °C and a strain rate of 0.11 s^{-1} in the edge-crack test. W_b decreased with increasing c_0 but with an abrupt drop at a characteristic c_0 value of $c_0^* \approx 1.8$ mm, in contrast to the continuous change in a non-SIC rubber (Fig. 2a). The force–displacement data used for the evaluation of W_b at each c_0 for NR-B are shown in the ESI.† The W_b–c_0 relationship was qualitatively similar to the observations for NR in earlier studies[36,46–48] and that shown in Fig. 1a. The c_0 dependence of G, calculated from the W_b data and eqn (2), shown in Fig. 3b indicates that G increases with increasing c_0 at $c_0 < c_0^*$, whereas G exhibits a discontinuous change at c_0^* and tends to become constant at a high c_0, which agrees qualitatively with Fig. 1b. Importantly, the data at $c_0 < c_0^*$ obey eqn (8), *i.e.*, $G = (c_0/B)^{1/2}/2$, as indicated by the solid line in the figure which is obtained using B as an adjustable parameter ($B = 3.65 \times 10^{-13}$ N^{-2} m^3). The dashed solid line depicts the result of eqn (8) using the B value ($B = 4.06 \times 10^{-13}$ N^{-2} m^3) which is separately evaluated

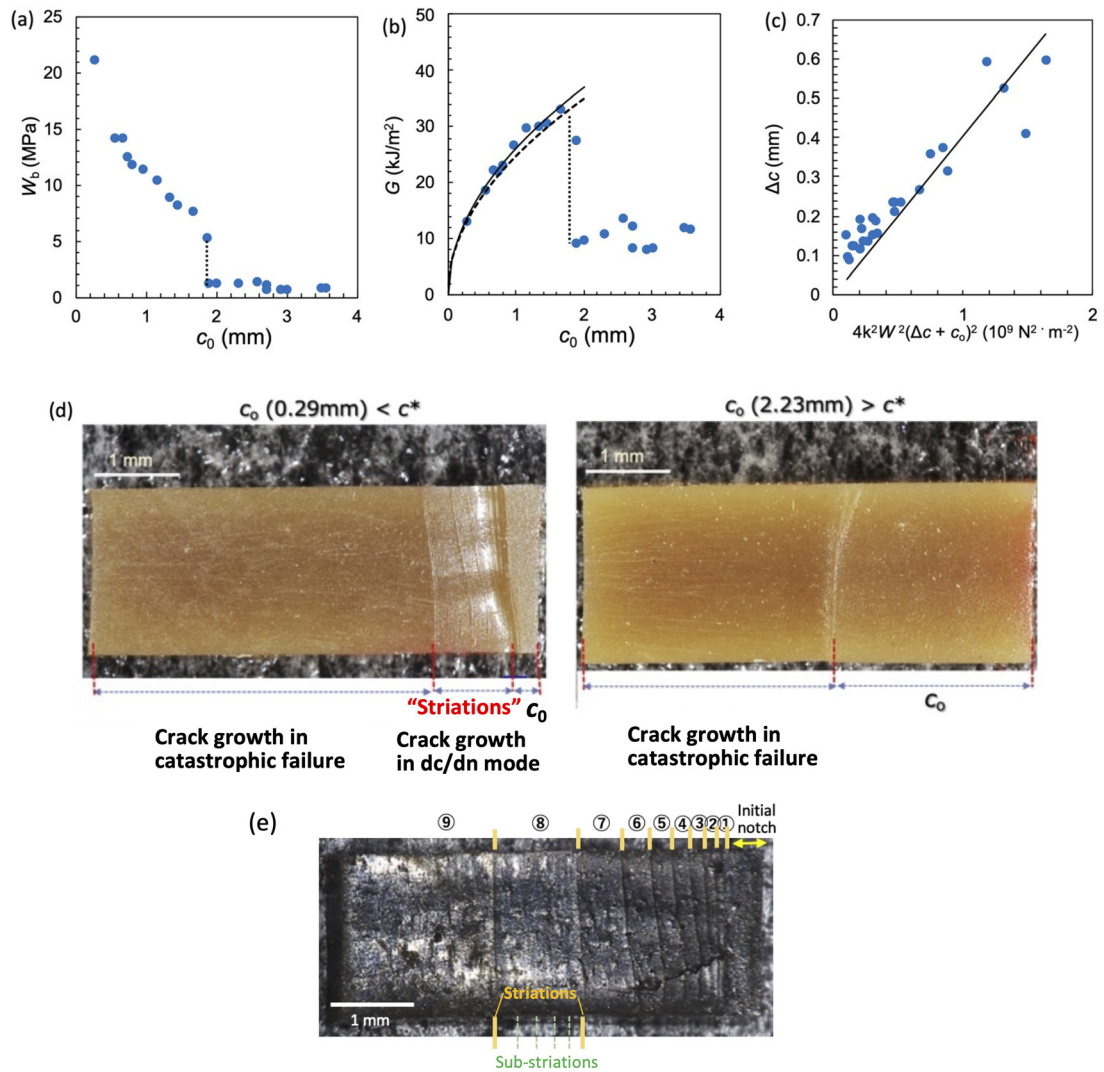

Fig. 3 (a) Strain energy density at break (W_b) as a function of the initial notch length (c_0) for NR-B at 25 °C and a strain rate of 0.11 s^{-1} in the edge-crack test. (b) The c_0 dependence of tearing energy (G) calculated using the data in (a) with eqn (2). The dashed line indicates the position of c_0^* at which an abrupt change occurs. The solid line represents the fitted curve of eqn (8) to the data using $B = 3.65 \times 10^{-13}$ N^{-2} m^3. The dashed solid line depicts the curve of eqn (8) with the B value (4.06×10^{-13} N^{-2} m^3) obtained using the cyclic loading test for the same specimen. (c) Increment of crack length (Δc) as a function of $4k^2B$ $(c_0 + \Delta c)^2$ W^2 for NR-B in the cyclic loading test. The line indicates the result of the linear regression. The slope corresponds to the B value (4.06×10^{-13} N^{-2} m^3). (d) Fracture surfaces for NR-B of $c_0 = 0.29$ mm ($< c_0^*$) and $c_0 = 2.23$ mm ($> c_0^*$). For $c_0 = 0.29$ mm, the fine striation lines characteristic of the crack growth *via* the dc/dn mode are observed. The zone "c_0" indicates the initial notch area. (e) Fracture surfaces including the striations for NR-B in the cyclic loading test.

from the cyclic loading test for the same NR-B specimen at 25 °C: the B value is obtained using eqn (6) from the slope of the linear regression in the plots of Δc *versus* $4k^2(c_0 + \Delta c)^2 W^2$ (Fig. 3c). The B value obtained by the cyclic loading test satisfactorily agrees with the B value fitted to the G–c_0 data, indicating without ambiguity that the fracture at $c_0 < c_0^*$ proceeds similarly to the crack growth under cyclic loading.

The different rupture modes at $c_0 > c_0^*$ and $c_0 < c_0^*$ are also appreciable when comparing the fracture surfaces of the corresponding specimens, as shown in Fig. 3d. The fracture surface of the edge-crack specimen with $c_0 = 0.29$ mm ($< c_0^*$) has characteristic marks (fine striation lines) that show the positions of the crack tip during the incremental growth of a crack. Similar striations are observed in the failure surfaces of NR in the cyclic fatigue tests,[19,20] and Fig. 3e shows the striations accompanied by the sub-striations in the failure surface of NR-B in the cyclic loading tests. As the corresponding features are not observed in the non-SIC rubbers, they are attributed to SIC.[19,20] The fracture surface of the edge-crack specimen of $c_0 = 2.23$ mm ($> c_0^*$) has no indication of striation (Fig. 3d). The fracture surface including the striations at $c_0 < c_0^*$ in the edge-crack tests indicates that SIC postpones the catastrophic crack growth.

The successful fit of eqn (8) to the G–c_0 data using the B value obtained by the cyclic loading test (Fig. 3b) and the striation characteristic of the cyclic crack growth (Fig. 3d) validate the theoretical interpretation of the data described in the previous section. The considerably different G–c_0 relationships beyond and above c_0^* are attributed to a transition of the rupture mode. The rupture at $c_0 > c_0^*$ without significant SIC near the crack tip is governed by the ordinary tear mode. At $c_0 < c_0^*$, the crack grows through a sufficiently large crystalline region, and the corresponding fracture proceeds similarly to the crack growth under cyclic loading, characterized by eqn (8). The maximum G value at c_0^* in Fig. 3b is considered a measure of the tearing energy enhanced by SIC (G_{SIC}). The quasi-plateau G value at $c_0 > c_0^*$ is regarded as a critical tearing energy for the onset of catastrophic crack growth without the SIC effect (G_T). In Fig. 3b, the G_{SIC} is evaluated to be 33 kJ m^{-2}, while the G_T is estimated to be 10 kJ m^{-2} from the average of the data at $c_0 > c_0^*$.

Effect of ambient temperature T

Fig. 4a and 5a show the c_0 dependence of W_b at various ambient temperatures (T) for NR-A and IR-A, respectively. A discontinuous gap in W_b at c_0^* is observed at a sufficiently low T, and c_0^* decreases with increasing T for both NR and IR. Importantly, no discontinuous change in W_b occurs when T exceeds a characteristic temperature (T^*), and the T^* values for NR and IR are appreciably different and are estimated to be 80 and 60 °C, the highest temperature at which the abrupt change of W_b is observed. At $T > T^*$ the SIC kinetics is so slow that SIC cannot occur sufficiently at $\dot{\varepsilon}$ of interest to enhance the tearing energy.

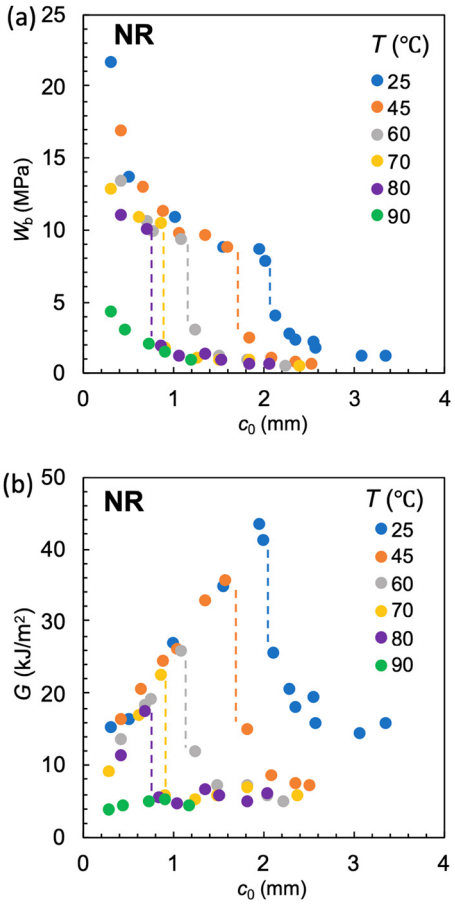

Fig. 4 (a) Strain energy density at break (W_b) as a function of the initial notch length (c_0) at various ambient temperatures (T) for NR-A at a strain rate of 0.5 s^{-1}. (b) The c_0 dependence of tearing energy (G) calculated using the data in (a) with eqn (2). The dashed lines indicate the position of c_0^* at which an abrupt change occurs for each T. No abrupt change is observed at 90 °C.

The G *vs.* c_0 plots obtained using eqn (2) and the data in Fig. 4a and 5a are shown in Fig. 4b and 5b, respectively. At $T < T^*$, the G values have the maximum at c_0^*, allowing the evaluation of the G_{SIC} at each T. G_{SIC} tends to decrease with increasing T in both NR and IR. At $T > T^*$, only G_T is obtained, reflecting the absence of an appreciable SIC effect. In contrast to G_{SIC}, G_T is almost independent of T at $T \geq 45$ °C. Thus, this method reveals the upper limit temperature (T^*), beyond which the effect of SIC on tearing energy vanishes, and the T-dependence of G_{SIC}. The G data in the vicinity of c_0^* at $c_0 > c_0^*$ in $T < T^*$ tend to be larger than the G_T value obtained at a high c_0. This tendency implies that a subtle degree of the SIC effect may exist at c_0 slightly beyond c_0^* although most of the effect vanishes when c_0 exceeds c_0^*.

Fig. 6 shows the plots of G_{SIC} and G_T obtained in Fig. 4b and 5b against T for NR-A and IR-A. The G_T values are nearly insensitive to T, except for the data at 25 °C, and there is no appreciable difference between these two rubbers. In contrast, for each rubber, the G_{SIC} value at a given T is several times larger than G_T, whereas G_{SIC} decreases with increasing T. These

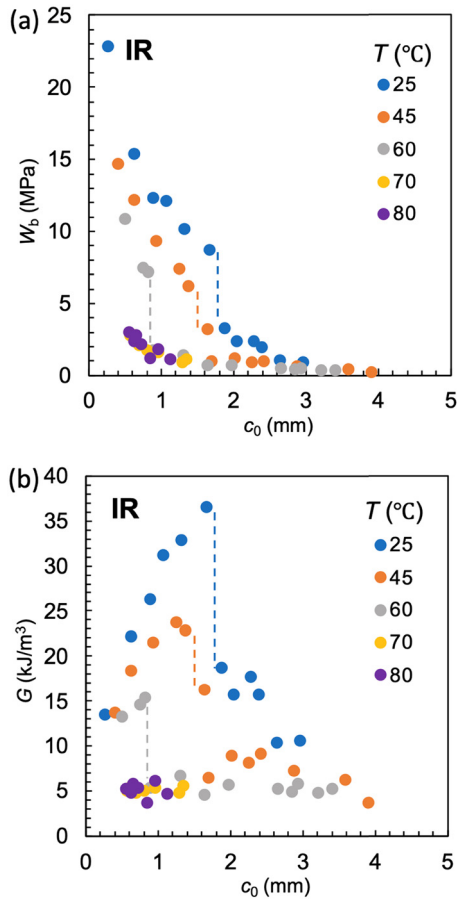

Fig. 5 (a) Strain energy density at break (W_b) as a function of the initial notch length (c_0) at various ambient temperatures (T) for IR-A at a strain rate of 0.5 s^{-1}. (b) The c_0 dependence of tearing energy (G) calculated using the data in (a) with eqn (2). The dashed lines indicate the position of c_0^* at which an abrupt change occurs for each T. No abrupt change is observed at $T \geq 70$ °C.

results indicate that G is significantly enhanced by hardening *via* SIC near the crack tip, whereas this reinforcement effect decreases with a decreasing crystallinity index. Notably, these two rubbers are considerably different in T^* and G_{SIC}; T^* for NR-A (80 °C) is approximately 20 °C higher than that for IR-A (60 °C), indicating that the reinforcement effect in NR emerges in a broader temperature range. Furthermore, the G_{SIC} value for NR at each T is significantly larger than that for IR.

The effects of T on SIC are separately investigated using WAXS experiments using unnotched bulk NR-A and IR-A specimens. Fig. 7a and b show the peak area of the crystal (200) diffraction (I_{200}) as a function of tensile strain at various T values. The evolution of I_{200} beyond the threshold strain reflects a continuous increase in the crystallinity index *via* SIC. The SIC onset strain (ε_{SIC}) was estimated from the onset of the evolution of I_{200}. For both rubbers, as T increases, ε_{SIC} increases, and I_{200} decreases when compared at a given strain. At a sufficiently high T, I_{200} remains zero over the entire strain range, indicating no occurrence of SIC; SIC can no longer be observed even at a high strain at 110 and 80 °C for NR-A and IR-A, respectively, which explains no occurrence of significant SIC at the crack tip in the edge-crack specimens at $T > T^*$.

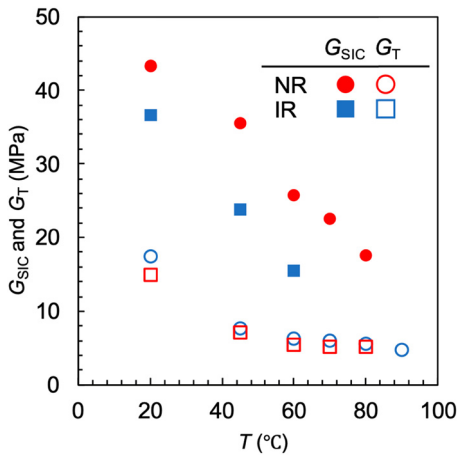

Fig. 6 Temperature dependence of the tearing energy *via* the SIC-reinforcement effect (G_{SIC}) and the tearing energy in catastrophic failure (G_T) for NR-A and IR-A. The SIC-reinforcement effect vanishes at $T >$ 80 °C and $T >$ 60 °C for NR-A and IR-A, respectively.

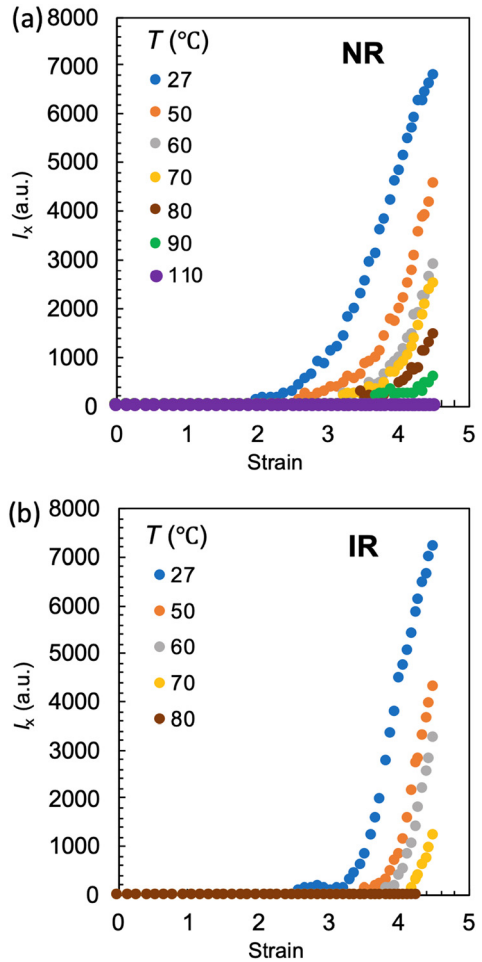

Fig. 7 Scattering intensity of the (200) diffraction of the SIC crystal as a function of the imposed tensile strain for (a) NR-A and (b) IR-A at various ambient temperatures.

The upper-limit temperature for SIC (T^*_{WAXS}), the highest temperature for the finite evolution of I_{200}, is evaluated to be 90 and 70 °C for NR-A and IR-A, respectively. The T^*_{WAXS} for NR-A is approximately 20 °C higher than that for IR-A, which is comparable to the difference in T^* (Fig. 6). This agreement validates the evaluation of T^* as the upper-limit ambient temperature in edge-crack tests. For each rubber, T^* is slightly lower than T^*_{WAXS}, probably because of the finite difference in the magnitudes of the effective strain and strain rate in the two measurements; the local strain and strain rate around the crack tip are higher than those in the tensile test of the unnotched bulk specimens. In addition, T^*_{WAXS} detects the threshold of SIC at the molecular level, while T^* reflects the threshold of the SIC effect on macroscopic tearing energy. The emergence of the SIC effect on bulk mechanical properties requires a finite degree of crystallization. This also explains the relationship of $T^*_{WAXS} > T^*$ for each rubber.

In each rubber, I_{200} decreases with increasing T when compared at the same strain, indicating that the crystallinity index at a given strain decreases as T increases. This result explains why the G_{SIC} decreases with increasing T for each rubber (Fig. 6).

The effects of T on the SIC for NR and IR have been studied using in-situ WAXS experiments, mainly in the sustained state with a constant strain beyond ε_{SIC} or by analyzing the stress–strain relationships.[23–29] The reported values of the melting temperature of the SIC crystal (T_f) of IR range from 60 to more than 100 °C depending on the magnitude of the imposed constant strain. The T^*_{WAXS} value (70 °C) for IR-A falls within the range of the reported values.

Effect of strain rate $\dot{\varepsilon}$

Fig. 8a and 9a show the c_0 dependence of W_b on NR-A and IR-A at various strain rates ($\dot{\varepsilon}$). The ambient temperature is 25 °C. The G–c_0 relationships calculated from these data are shown in Fig. 8b and 9b. For NR and IR, the effects of $\dot{\varepsilon}$ on the W_b–c_0 and G–c_0 relationships are similar to those of T (Fig. 4 and 5). A discontinuous gap in W_b and G at c_0^* is observed at a sufficiently low $\dot{\varepsilon}$, and the c_0^* value decreases with increasing $\dot{\varepsilon}$. The discontinuous feature vanishes when $\dot{\varepsilon}$ exceeds the threshold value $\dot{\varepsilon}^*$. We regard the maximum G value at c_0^* as the G_{SIC} at each $\dot{\varepsilon}$, and the average of the quasi-plateau values at $c_0 > c_0^*$ as the G_T.

Fig. 10 shows the plots of G_{SIC} and G_T against $\dot{\varepsilon}$ for NR-A and IR-A. An appreciable reinforcement of SIC on tearing energy ($G_{SIC} > G_T$) is observed at $\dot{\varepsilon} < \dot{\varepsilon}^*$, while it vanishes at $\dot{\varepsilon} > \dot{\varepsilon}^*$. At $\dot{\varepsilon} > \dot{\varepsilon}^*$, the imposed strain rate is so high that the matrix around the crack tip cannot have enough time to undergo a sufficient degree of SIC, resulting in a catastrophic fracture governed by the G_T. As this result originates from the competition between the SIC and strain rate, $\dot{\varepsilon}^*$depends on T of interest. For convenience, we regard the $\dot{\varepsilon}^*$ from the highest $\dot{\varepsilon}$ value at which finite discontinuity is observed in the G–c_0 relationship because the data as a function of $\dot{\varepsilon}$ are discrete. Notably, the $\dot{\varepsilon}^*$ value for NR-A (50 s^{-1}) is considerably higher than that for IR-A (0.5 s^{-1}). There exists some uncertainty in the $\dot{\varepsilon}^*$ value for IR-A

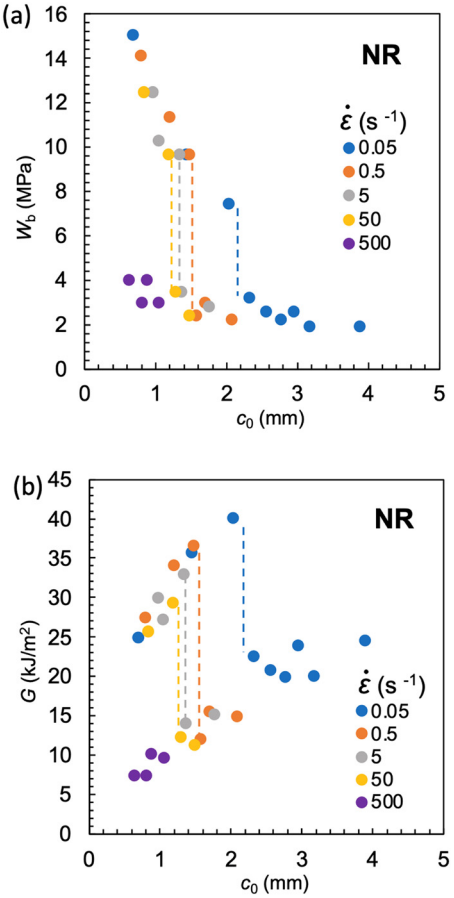

Fig. 8 (a) Strain energy density at break (W_b) as a function of the initial notch length (c_0) at various strain rates ($\dot{\varepsilon}$) for NR-A at 25 °C. (b) The c_0 dependence of tearing energy (G) calculated using the data in (a) with eqn (2). The dashed lines indicate the position of c_0^* at which an abrupt change occurs for each $\dot{\varepsilon}$. No abrupt change is observed at 500 s^{-1}.

because of the ambiguity of the discontinuous feature in the data at 5 s^{-1}: Finite discontinuity is appreciable in W_b (Fig. 9a) but not in G (Fig. 9b). The $\dot{\varepsilon}^*$ value for IR-A may be slightly higher than 0.5 s^{-1}. Nevertheless, we can conclude safely that $\dot{\varepsilon}^*$ for NR-A is at least one order of magnitude higher than that for IR-A because of a definite difference in the discontinuity in the data at 50 s^{-1} between them. In addition, the G_{SIC} for NR-A is larger than that for IR-A when compared at the same $\dot{\varepsilon}$. As in the case of the T effect (Fig. 6), the finite superiority of NR relative to IR in reinforcing ability *via* SIC is appreciable in the effect of $\dot{\varepsilon}$.

Several researchers have studied the effect of $\dot{\varepsilon}$ on SIC for NR or IR using *in situ* WAXS experiments.[31–35] Recently, Kitamura *et al.*[35] showed that the times required for the occurrence of finite SIC in NR and IR were comparable and less than 0.01 s. Candau *et al.*[34] also reported that the finite superiority of NR relative to IR in SIC ability (observed at slow strain rates) disappeared at high strain rates. According to their results, the occurrence of finite SIC and the disappearance of the difference in the reinforcement effect between NR and IR are expected at high strain rates of more than 100 s^{-1}. However, the $\dot{\varepsilon}^*$ values (50 s^{-1} for NR-A and 0.5 s^{-1} for IR-A) in the edge-crack

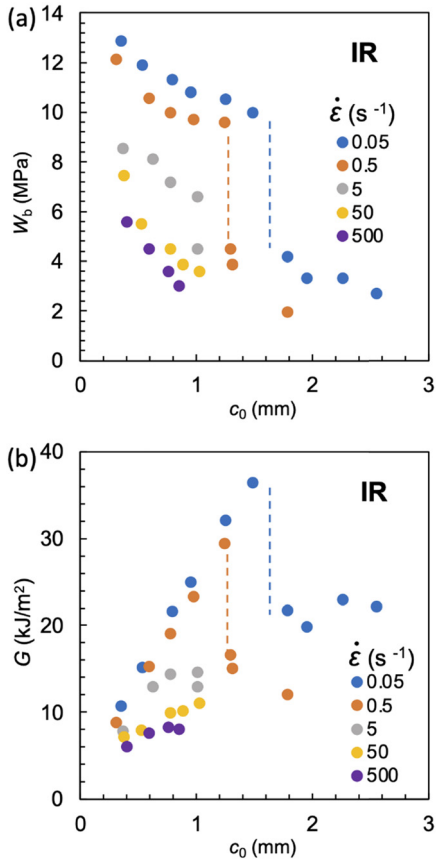

Fig. 9 (a) Strain energy density at break (W_b) as a function of the initial notch length (c_0) at various strain rates ($\dot{\varepsilon}$) for IR-A at 25 °C. (b) The c_0 dependence of tearing energy (G) calculated using the data in (a) with eqn (2). The dashed lines indicate the position of c_0^* at which an abrupt change occurs for each $\dot{\varepsilon}$. No abrupt change is observed at $\dot{\varepsilon} > 5$ s^{-1}.

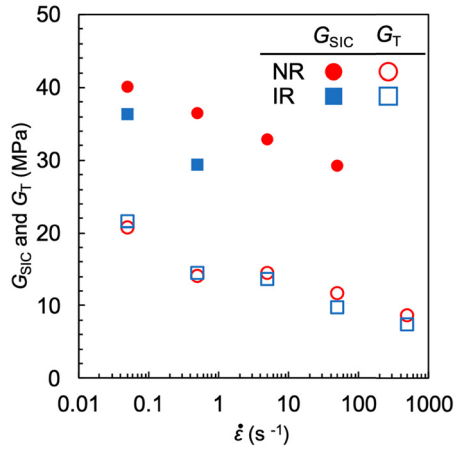

Fig. 10 Strain rate dependence of the tearing energy *via* the SIC-reinforcement effect (G_{SIC}) and the tearing energy in catastrophic failure (G_T) for NR-A and IR-A. The SIC-reinforcement effect vanishes at $\dot{\varepsilon} > 50$ s^{-1} and $\dot{\varepsilon} > 0.5$ s^{-1} for NR-A and IR-A, respectively.

tests are appreciably lower than this expectation, and they were considerably different between NR-A and IR-A. These discrepancies indicate that the threshold for the emergence of the SIC effect on the macroscopic mechanical strength (reflected in the edge crack tests) is different from the onset of SIC at the molecular level (detected by WAXS): the onset of the finite mechanical reinforcement effect requires a significant degree of crystallization. It should also be noted that the magnitudes of local strain and strain-rate near the crack tip are considerably larger than those in the unnotched bulk materials used in the WAXS measurements, when compared at the same degree of imposed macroscopic strain.

Summary

The present study demonstrates the availability of edge-crack tests to quantify the enhancement effect of SIC on tearing energy and its upper limits of T and $\dot{\varepsilon}$ for the emergence. In the edge-crack tests using the initial notch length (c_0) as a variable, the pre-notched SIC rubber specimens exhibit a discontinuous change in the strain energy density at break (W_b) at a characteristic c_0 value (c_0^*), as a result of the transition in the rupture mechanism between the ordinary tear mode, simply governed by G_T at $c_0 > c_0^*$, and the cyclic growth mode *via* a significant degree of SIC near the crack tip at $c_0 < c_0^*$. We validated the fracture *via* cyclic growth mode at $c_0 < c_0^*$ by confirming the distinctive relationship $G = (c_0/B)^{1/2}/2$, with the B value separately obtained using the cyclic loading test, and by observing the characteristic striations on the fracture surface.

The maximum G value at c_0^*, calculated from the W_b–c_0 data by extending Thomas' theory, is regarded as a measure of the tearing energy enhanced by SIC (G_{SIC}). The magnitude of the G_{SIC} is several times larger than that of the G_T, reflecting that the crack propagates through the matrix hardened by crystallization. The G_{SIC} values decrease with increasing T and $\dot{\varepsilon}$ due to a reduction in the crystallinity index. The upper limits of T and $\dot{\varepsilon}$ for the finite reinforcement effect *via* SIC (T^* and $\dot{\varepsilon}^*$, respectively) are evaluated from the vanishing points of the transition feature.

NR exhibits a higher magnitude of G_{SIC} at a given T or $\dot{\varepsilon}$ than IR, whereas these rubbers show no appreciable difference in G_T. NR has an approximately 20 °C higher value of T^* and at least one order of magnitude larger value of $\dot{\varepsilon}^*$ than IR. The WAXS measurements confirm a reduction in the crystallinity index with increasing T and an approximately 20 °C higher upper-limit temperature for the occurrence of SIC in NR. Comparisons using the G_{SIC}, T^*, and $\dot{\varepsilon}^*$ values reveal that NR is obviously superior to IR in the mechanical reinforcement effect *via* SIC.

Conflicts of interest

There are no conflicts to declare.

Acknowledgements

We appreciate Prof. James Busfield at the Queen Mary University of London for the fruitful discussion. This work

was partly supported by the JST, CREST grant number JPMJCR2091, Japan. The authors thank Ayano Kozono for her assistance in making the graphs.

References

1 J. E. Mark, B. Erman and C. M. Roland, *The Science and Technology of Rubber*, Academic Press, 2013.
2 G. R. Hamed, *Engineering with Rubber*, ed. A. N. Gent, Carl Hanser Verlag, Munich, 2012, p. 433.
3 S. Kohjiya and Y. Ikeda, *Chemistry, Manufacture and Applications of Natural Rubber*, Woodhead Publishing, 2nd edn, 2021.
4 J. R. Katz, Röntgenspektrographische Untersuchungen Am Gedehnten Kautschuk Und Ihre Mögliche Bedeutung Für Das Problem Der Dehnungseigenschaften Dieser Substanz, *Naturwissenschaften*, 1925, **13**(19), 410–416.
5 K. Brüning, *In-Situ Structure Characterization of Elastomers during Deformation and Fracture*, Springer, Cham, 2014.
6 A. N. Gent, S. Kawahara and J. Zhao, Crystallization and Strength of Natural Rubber and Synthetic Cis-1,4-Polyisoprene, *Rubber Chem. Technol.*, 1998, **71**(4), 668–678.
7 R. Clamroth and T. Kempermann, Comparison of Methods for the Determination of Tear Strength, *Polym. Test.*, 1986, **6**(1), 3–35.
8 M. Tosaka, S. Kohjiya, S. Murakami, S. Poompradub, Y. Ikeda, S. Toki, I. Sics and B. S. Hsiao, Effect of Network-Chain Length on Strain-Induced Crystallization of NR and IR Vulcanizates, *Rubber Chem. Technol.*, 2004, **77**(4), 711–723.
9 S. Trabelsi, P.-A. Albouy and J. Rault, Stress-Induced Crystallization Properties of Natural and Synthetic CIS-Polyisoprene, *Rubber Chem. Technol.*, 2004, **77**(2), 303–316.
10 Y. Tanaka, Structural Characterization of Natural Polyisoprenes: Solve the Mystery of Natural Rubber Based on Structural Study, *Rubber Chem. Technol.*, 2001, **74**(3), 355–375.
11 J. Che, C. Burger, S. Toki, L. Rong, B. S. Hsiao, S. Amnuaypornsri and J. Sakdapipanich, Crystal and Crystallites Structure of Natural Rubber and Synthetic Cis-1,4-Polyisoprene by a New Two Dimensional Wide Angle X-Ray Diffraction Simulation Method. I. Strain-Induced Crystallization, *Macromolecules*, 2013, **46**(11), 4520–4528.
12 M. Oouchi, J. Ukawa, Y. Ishii and H. Maeda, Structural Analysis of the Terminal Groups in Commercial Hevea Natural Rubber by 2D-NMR with DOSY Filters and Multiple-WET Methods Using Ultrahigh-Field NMR, *Biomacromolecules*, 2019, **20**(3), 1394–1400.
13 M. Dixit and T. Taniguchi, Substantial Effect of Terminal Groups in Cis-Polyisoprene: A Multiscale Molecular Dynamics Simulation Study, *Macromolecules*, 2022, **55**(21), 9650–9662.
14 C. Liu, N. Morimoto, L. Jiang, S. Kawahara, T. Noritomi, H. Yokoyama, K. Mayumi and K. Ito, Tough Hydrogels with Rapid Self-Reinforcement, *Science*, 2021, **372**(6546), 1078–1081.
15 W. V. Mars and A. Fatemi, Factors That Affect the Fatigue Life of Rubber: A Literature Survey, *Rubber Chem. Technol.*, 2004, **77**(3), 391–412.
16 N. Saintier, G. Cailletaud and R. Piques, Cyclic Loadings and Crystallization of Natural Rubber: An Explanation of Fatigue Crack Propagation Reinforcement under a Positive Loading Ratio, *Mater. Sci. Eng., A*, 2011, **528**(3), 1078–1086.
17 P. Rublon, B. Huneau, E. Verron, N. Saintier, S. Beurrot, A. Leygue, C. Mocuta, D. Thiaudière and D. Berghezan, Multiaxial Deformation and Strain-Induced Crystallization around a Fatigue Crack in Natural Rubber, *Eng. Fract. Mech.*, 2014, **123**, 59–69.
18 F. Xiang, K. Schneider and G. Heinrich, New Observations Regarding Fatigue Crack Paths and Their Fracture Surfaces in Natural Rubber: Influences of R-Ratio and Pre-Load, *Int. J. Fatigue*, 2020, **135**, 105508.
19 J.-B. Le Cam and E. Toussaint, The Mechanism of Fatigue Crack Growth in Rubbers under Severe Loading: The Effect of Stress-Induced Crystallization, *Macromolecules*, 2010, **43**(10), 4708–4714.
20 B. Ruellan, J.-B. Le Cam, E. Robin, I. Jeanneau, F. Canévet, G. Mauvoisin and D. Loison, Fatigue Crack Growth in Natural Rubber: The Role of SIC Investigated through Post-Mortem Analysis of Fatigue Striations, *Eng. Fract. Mech.*, 2018, **201**, 353–365.
21 S. Trabelsi, P.-A. Albouy and J. Rault, Stress-Induced Crystallization around a Crack Tip in Natural Rubber, *Macromolecules*, 2002, **35**(27), 10054–10061.
22 Q. Demassieux, D. Berghezan and C. Creton, *Microfocused Beam SAXS and WAXS Mapping at the Crack Tip and Fatigue Crack Propagation in Natural Rubber BT – Fatigue Crack Growth in Rubber Materials: Experiments and Modelling*, ed. G. Heinrich, R. Kipscholl, R. Stoček, Springer International Publishing, Cham, 2021, pp. 467–491.
23 J. Rault, J. Marchal, P. Judeinstein and P. A. Albouy, Stress-Induced Crystallization and Reinforcement in Filled Natural Rubbers: 2H NMR Study, *Macromolecules*, 2006, **39**(24), 8356–8368.
24 S. Toki, I. Sics, B. S. Hsiao, M. Tosaka, S. Poompradub, Y. Ikeda and S. Kohjiya, Probing the Nature of Strain-Induced Crystallization in Polyisoprene Rubber by Combined Thermomechanical and *In Situ* X-Ray Diffraction Techniques, *Macromolecules*, 2005, **38**(16), 7064–7073.
25 P.-A. Albouy, J. Marchal and J. Rault, Chain Orientation in Natural Rubber, Part I: The Inverse Yielding Effect, *Eur. Phys. J. E: Soft Matter Biol. Phys.*, 2005, **17**(3), 247–259.
26 Y. Miyamoto, H. Yamao and K. Sekimoto, Crystallization and Melting of Polyisoprene Rubber under Uniaxial Deformation, *Macromolecules*, 2003, **36**(17), 6462–6471.
27 N. Candau, R. Laghmach, L. Chazeau, J.-M. Chenal, C. Gauthier, T. Biben and E. Munch, Temperature Dependence of Strain-Induced Crystallization in Natural Rubber: On the Presence of Different Crystallite Populations, *Polymer*, 2015, **60**, 115–124.
28 P. Chen, J. Zhao, Y. Lin, J. Chang, L. Meng, D. Wang, W. Chen, L. Chen and L. Li, In Situ Characterization of

Strain-Induced Crystallization of Natural Rubber by Synchrotron Radiation Wide-Angle X-Ray Diffraction: Construction of a Crystal Network at Low Temperatures, *Soft Matter*, 2019, **15**(4), 734–743.

29 N. Candau, R. Laghmach, L. Chazeau, J.-M. Chenal, C. Gauthier, T. Biben and E. Munch, Influence of Strain Rate and Temperature on the Onset of Strain Induced Crystallization in Natural Rubber, *Eur. Polym. J.*, 2015, **64**, 244–252.

30 P. J. Flory, Thermodynamics of Crystallization in High Polymers. I. Crystallization Induced by Stretching, *J. Chem. Phys.*, 1947, **15**(6), 397–408.

31 K. Brüning, K. Schneider, S. V. Roth and G. Heinrich, Kinetics of Strain-Induced Crystallization in Natural Rubber Studied by WAXD: Dynamic and Impact Tensile Experiments, *Macromolecules*, 2012, **45**(19), 7914–7919.

32 B. N. J. Persson, O. Albohr, G. Heinrich, H. Ueba, C.-Y. Hui, A. Jagota, S. J. Bennison and J. D. Londono, Crack Propagation in Rubber-like Materials, *J. Phys.: Condens. Matter*, 2005, **459**(2034), 1489–1516.

33 M. Tosaka, K. Senoo, K. Sato, M. Noda and N. Ohta, Detection of Fast and Slow Crystallization Processes in Instantaneously-Strained Samples of Cis-1,4-Polyisoprene, *Polymer*, 2012, **53**(3), 864–872.

34 N. Candau, L. Chazeau, J.-M. Chenal, C. Gauthier and E. Munch, A Comparison of the Abilities of Natural Rubber (NR) and Synthetic Polyisoprene Cis-1,4 Rubber (IR) to Crystallize under Strain at High Strain Rates, *Phys. Chem. Chem. Phys.*, 2016, **18**(5), 3472–3481.

35 Y. Kitamura, K. Okada, H. Masunaga and M. Hikosaka, Role of Strain Rate in the Strain-Induced Crystallization (SIC) of Natural and Synthetic Isoprene Rubber, *Polym. J.*, 2019, **51**(2), 221–226.

36 C. L. M. Bell, D. Stinson and A. G. Thomas, Measurement of Tensile Strength of Natural Rubber Vulcanizates at Elevated Temperature, *Rubber Chem. Technol.*, 1982, **55**(1), 66–75.

37 R. S. Rivlin and A. G. Thomas, Rupture of Rubber. I. Characteristic Energy for Tearing, *J. Polym. Sci.*, 1953, **10**(3), 291–318.

38 H. W. Greensmith, Rupture of Rubber. IV. Tear Properties of Vulcanizates Containing Carbon Black, *J. Polym. Sci.*, 1956, **21**(98), 175–187.

39 G. J. Lake, C. C. Lawrence and A. G. Thomas, High-Speed Fracture of Elastomers: Part I, *Rubber Chem. Technol.*, 2000, **73**(5), 801–817.

40 J. R. Rice, A Path Independent Integral and the Approximate Analysis of Strain Concentration by Notches and Cracks, *J. Appl. Mech.*, 1968, **35**(2), 379–386.

41 S.-J. Chang, Path-Independent Integral for Rupture of Perfectly Elastic Materials, *Z. Angew. Math. Phys.*, 1972, **23**(1), 149–152.

42 Y. Qi, J. Caillard and R. Long, Fracture Toughness of Soft Materials with Rate-Independent Hysteresis, *J. Mech. Phys. Solids*, 2018, **118**, 341–364.

43 R. Long, C.-Y. Hui, J. P. Gong and E. Bouchbinder, The Fracture of Highly Deformable Soft Materials: A Tale of Two Length Scales, *Annu. Rev. Condens. Matter Phys.*, 2021, **12**(1), 71–94.

44 E. Elmukashfi, An Experimental Method for Estimating the Tearing Energy in Rubber-like Materials Using the True Stored Energy, *Sci. Rep.*, 2021, **11**(1), 16229.

45 C. Creton and M. Ciccotti, Fracture and Adhesion of Soft Materials: A Review, *Rep. Prog. Phys.*, 2016, **79**(4), 46601.

46 A. G. Thomas, Fracture of Rubber, *The Physical Basis of Yield and Fracture Conference Proceedings*, Oxford, 1967, p. 134.

47 A. G. Thomas and J. M. Whittle, Tensile Rupture of Rubber, *Rubber Chem. Technol.*, 1970, **43**(2), 222–228.

48 G. Rong, G. R. Hamed and J. Jiang, Comparison of the Strength of Normal and Edge-Cut Tensile Specimens of Styrene-Butadiene Rubber and Natural Rubber with Similar Crosslink Density, *Rubber Chem. Technol.*, 2016, **89**(4), 631–639.

49 G. R. Hamed and N. Rattanasom, Effect of Crosslink Density on Cut Growth in Black-Filled Natural Rubber Vulcanizates, *Rubber Chem. Technol.*, 2002, **75**(5), 935–942.

50 G. R. Hamed and B. H. Park, The Mechanism of Carbon Black Reinforcement of SBR and NR Vulcanizates, *Rubber Chem. Technol.*, 1999, **72**(5), 946–959.

51 A. G. Thomas, Rupture of Rubber. V. Cut Growth in Natural Rubber Vulcanizates, *J. Polym. Sci.*, 1958, **31**(123), 467–480.

52 G. R. Hamed, Effect of Crosslink Density on the Critical Flaw Size of a Simple Elastomer, *Rubber Chem. Technol.*, 1983, **56**(1), 244–251.

53 P. Paris and F. Erdogan, A Critical Analysis of Crack Propagation Laws, *J. Basic Eng.*, 1963, **85**(4), 528–533.

54 A. N. Gent, P. B. Lindley and A. G. Thomas, Cut Growth and Fatigue of Rubbers. I. The Relationship between Cut Growth and Fatigue, *J. Appl. Polym. Sci.*, 1964, **8**(1), 455–466.

55 P. J. Flory and J. Rehner, Statistical Mechanics of Cross-Linked Polymer Networks II Swelling, *J. Chem. Phys.*, 1943, **11**(11), 521–526.

